Supplementary Material

The 'Photosynthetic C_1 pathway' links carbon assimilation and growth in California poplar

Kolby J. Jardine[*1], Luiza Gallo[1,2], Melissa Roth[3], Shivani Upadhyaya[3], Trent Northen[4], Suzanne Kosina[4], Guillaume Tcherkez[5,6], Aymerick Eudes[4], Tomas Domigues[2], Markus Greule[7], Suman Som[1], and Frank Keppler[7,8]

[1*]Lawrence Berkeley National Laboratory, Climate and Ecosystem Sciences Division, Berkeley, CA, USA (corresponding author email: kjjardine@lbl.gov)

[2]University of São Paulo, FFCLRP, Dept. of Biology, Ribeirão Preto, SP, Brazil

[3]University of California Berkeley, Dept. of Plant and Microbial Biology, Berkeley, CA, USA

[4]Lawrence Berkeley National Laboratory, Environmental Genomics and Systems Biology Division, Berkeley, CA, USA

[5]Australian National University, Division of Plant Sciences, Research School of Biology, Canberra, Australia

[6]Institut de Recherche en Horticulture et Semences, INRAE, Université d'Angers, 49070 Beaucouzé, France

[7]Institute of Earth Sciences, Heidelberg University, Im Neuenheimer Feld 234-236, D-69120 Heidelberg, Germany

[8]Heidelberg Center for the Environment HCE, Heidelberg University, D-69120 Heidelberg, Germany

Supplementary Information Content

Supplementary Notes

Supplementary Figures

of a *P. trichocarpa* individual in the Berkeley, CA field site during the late growing season (April 20233), under constant light, C_a, and reference humidity.

- **Figure S16**: Time series plot showing the diurnal variation of (**a**) leaf photosynthesis (A_{net}), stomatal conductance (g_s), and water potential (LWP) together with (**b**) leaf transpiration (E), methanol emissions (CH_3OH), and temperature versus hr of the day from the canopy of a *P. trichocarpa* individual in the Berkeley, CA field site during the late growing season (June 20233), under constant light, C_a, and reference humidity.
- **Figure S17**: Graphical representation of diurnal growth and methanol emission processes in plants. Created in BioRender. *K. Jardine*. (2024) *BioRender.com/r65a877*
- **Figure S18:** Graphical summary of gas exchange methods used during $^{13}CO_2$ labelling of the photosynthetic C_1 pathway in *P. trichocharpa* leaves at the (a) leaf level on detached and hydrated branches lasting 1-5 hrs and (b) branch level using potted plants lasting 2-5 days. *Created in BioRender. K. Jardine (2024) BioRender.com/d79c177*

Supplementary References

Supplementary Notes

Note 1: **Pectin demethylation, methanol emissions, and growth**

In *A. thaliana*, increases in tissue elasticity in living meristems correlated with pectin demethylesterification[1] which is required for the initiation of organ formation[2]. When pectin demethylation was inhibited, stiffening of the cell walls throughout the meristem blocked the formation of primordia. Thus, pectin demethylation is a critical process that regulates the direction and speed of cell wall expansion during growth and morphogenesis[3]. Recent studies have revealed that nanofilaments of pectin homogalacturonan in the primary cell wall shift between crystalline and anisotropic phases depending on their methylation status. Thus, complex cell shapes and polarized cell expansion patterns can derive from pectin demethylation without turgor-driven growth[4]. During its biosynthesis, pectin is highly methyl esterified in the Golgi using AdoMet as the methyl donor prior to export and incorporation into the growing cell wall[5]. Methanol production and emission by plants has been highly correlated with leaf expansion rates[6] with young rapidly growing leaves consistently observed to have higher methanol emissions rates than slower growing mature leaves[6-8]. When a global atmospheric budget of methanol was developed, methanol was found to be the second most abundant volatile organic compound in the atmosphere only behind methane[9], with the majority (62%) of the annual 206 Tg yr^{-1} source to the atmosphere deriving from plant growth. However, given the large reservoir of methylated pectin in leaves and other plant tissues, leaf methanol emissions are assumed to have no direct connection with photosynthesis with methanol emissions continuing in the dark, related to growth processes[10]. This is in contrast with isoprene emissions which are not stored in plants, and produced within mins of leaf light exposure, requiring both C_3 carbon skeletons from the Calvin-Benson cycle and ATP and NADPH from the light reactions[11]. However, trees are well known to mainly grow at night due to reduced turgor pressure associated with high rates of transpiration[12], while photosynthesis only occurs during the day due to the strict light requirement. While isoprene emissions at night are regularly negligible, to date, leaf methanol emission studies at night have been obscured by stomatal closure at night in most species investigated. Large emission bursts of methanol are typically observed at sunrise as stomata open[13,14], suggesting continued growth and methanol production at night. In the current study, we leveraged the high stomatal conductance of *P. trichocarpa* at night to study diurnal methanol emission and growth dynamics.

Note 2: **Biochemical steps of the 'Photosynthetic C_1 pathway'**

A proposed biochemical model is presented integrating CO_2 fixation by the Calvin-Benson cycle with the 'Photosynthetic C_1 pathway' involving seven distinct enzymatic steps in the chloroplast followed by AdoMet regeneration in the cytosol (see **Figures 5-6** in the main text) as a major source of cellular methyl transfer reactions in the light and the main cause of the large natural carbon isotope anomaly in the major leaf C_1 pools. The photosynthetic C_1 pathway is initiated by the same enzyme that initiates the dark reactions of the Calvin-Benson cycle, RuBisCO. Catalyzation of the carboxylation of ribulose-1,5-biphosphate with CO_2 by RuBisCO leads to the formation of 3-phosphoglceric acid (3PGA), which is processed by the Calvin-Benson cycle to

regenerate ribulose 1,5-biphosphate. 3PGA is subsequently converted to serine via the activity of the three enzymes of the phosphorylated serine pathway in chloroplasts including 3-phosphoglycerate dehydrogenase (PGDH), 3-phosphoserine aminotransferase (PSAT) and 3-phosphoserine phosphatase (PSP). Following the formation of serine, the C_1 carbon atom is used as a methyl donor in the formation of the 5,10-methylene-THF intermediate catalyzed by serine hydroxymethyltransferase (SHMT). Following reduction of 5,10-methylene-THF to 5-methyl-THF by methylenetetrahydrofolate reductase (MTHFR), the 5-methyl group is transferred by a chloroplastic methionine synthase (MS) to homocysteine to form methionine, the end product of the photosynthetic C_1 pathway. The genomes of most land plant species encode several MTHFR isoforms which lack an obvious target sequence[15], suggesting the MTHFR subcellular localization in algae and land plant species is the cytosol[16]. However, it is important to keep in mind that MTHFR is the least understood enzyme of THF-mediated one-carbon metabolism in plants[15] and its subcellular location(s) require additional research. Here, we consider that 5-methyl-THF synthesis catalyzed by MTHFR occurs in the cytosol, with the export of 5,10-methylene-THF out of chloroplasts together with 5-methyl-THF import into chloroplasts mediated by one or more chloroplastic folate transporters[17].

Ensuing the export of methionine to the cytosol, it is activated to AdoMet via reaction with ATP catalyzed by methionine adenosyltransferase (MAT). AdoMet is subsequently imported into numerous organelles[18] and utilized to sustain a potentially large flux of methyl transfer reactions targeting a broad spectrum of substrates from nucleic acids, lipids, proteins, carbohydrates, and small metabolites[19] catalyzed by a large family of AdoMet-dependent methyltransferases[20]. Following the methyl transfer to the substrate and formation of S-adenosyl-homocysteine intermediate, homocysteine and ATP are regenerated following the reaction catalyzed by S-adenosyl-homocysteine hydrolase (SAHH). Importantly, during this photosynthetic C_1 pathway, carbon atoms that were recently assimilated by RuBisCO and the Calvin-Benson cycle as CO_2 are rapidly activated to the universal methyl donor group in AdoMet before being transferred to numerous target substrates. This implies that, despite potentially supporting many cellular methylations at high rates, methionine concentrations, as well as other intermediates of the pathway, are not required to accumulate to high levels to support a high C_1 flux. Instead, we suggest that high rates of cellular methylation reactions could be supported by a high rate of methionine turnover as well as export to other tissues via phloem loading.

Note 3: Large, natural, and universal ^{13}C depletion of plant C_1 pools

Consistent with the existence of a photosynthetic C_1 pathway in plants are the findings of a large natural ^{13}C-isotope anomaly in the terrestrial plant C_1 carbon pool[21]. Twenty years ago, it was discovered that the most abundant C_1 units of terrestrial plants, the methyl ester groups of pectin and methoxyl groups in lignin, have a stable carbon isotope signature exceptionally, and naturally depleted in ^{13}C. For example, while atmospheric CO_2 has an isotopic signature of around -8.5 ‰, isotopic discrimination against $^{13}CO_2$ during diffusion into leaves and carboxylation reactions

catalyzed by RuBisCO results in stable carbon isotopic composition naturally depleted in ^{13}C (i.e. average C_3 biomass has a $\delta^{13}C$ value of -27.0‰ VPDB[22]). RuBisCO is well characterized to catalyze carboxylation of ribulose-1,5-biophosphate with a strong kinetic isotope effect, such that $^{12}CO_2$ is assimilated slightly faster than $^{13}CO_2$[23]. Recently direct in vitro measurements with NMR confirm that the last enzyme of the photosynthetic C_1 pathway, methionine synthase, catalyzes the transfer of the methyl group from 5-methyl-THF to homocysteine with a strong normal ^{13}C kinetic isotope effect during methionine synthesis only on the S-methyl group of methionine of ~20‰[24]. While the cause of the natural ^{13}C-isotopic anomaly in the leaf C_1 pool remains unclear, we propose that the sequential events of natural discrimination against ^{13}C during CO_2 diffusion and carboxylation by RuBisCO followed by methionine synthesis as the last step of the photosynthetic C_1 pathway imparts an extremely ^{13}C-depleted carbon isotope signature on the S-methyl group of methionine, and consequently all substrates that receive C_1 carbon during their synthesis or regulation via methyl transfer from AdoMet following activation of Methionine with ATP. Thus, we suggest that the photosynthetic C_1 pathway may be responsible for the large carbon isotope anomaly observed in major leaf C_1 carbon pools[21]. Moreover by connecting carbon assimilation in leaves with growth in other tissues, the results also suggest that phloem loading and transport of methionine[25] and S-methymethionine[26] may play quantitatively important, but poorly understood roles in plant growth and development[27].

Note S4: Methanol emission: a metabolic biomarker of plant physiological status?

At midnight, when the leaf water potential recovered (-0.2 +/- 0.1 MPa) from afternoon values (-1.1 +/- 0.2 MPa), branch emissions of both ^{12}C-methanol and ^{13}C-methanol increased steadily throughout the night (see **Figure 1** in the main text and supplementary **Figures S1-5**), despite leaf temperature and transpiration slowly decreasing. One possible explanation for these trends is hydraulically-driven growth acceleration associated with increasing cell turgor pressure throughout the night as plant water storage capacity is refilled. Consistent with previous studies from physical measurements that suggest trees mainly grow at night and in the early morning[12], diurnal observations of methanol emissions suggest an accelerated growth phase starting around midnight and ending midday followed by a decelerated growth period from midday to midnight. Thus, growth and methanol production may be linked with the recovery of leaf water reservoirs at night, and accelerate with the rise in temperature in the morning. Due to high transpiration rates in the morning that leads to declining leaf water potentials, this is followed by a decelerated growth phase between midday and midnight, where growth and methanol emissions may be suppressed by increased tissue water stress in the afternoon and also negatively influenced by declining temperatures throughout the evening. The decline in branch methanol emissions in the early afternoon observed in the field experiment prior to the decline in photosynthesis and transpiration (i.e. supplementary **Figure S13**) is consistent with similar findings in a recent controlled drought experiment[28]. However, unlike at night when changes in growth rates rather than stomatal conductance can be attributed to the increase in methanol emissions throughout the night, afternoon decreases in methanol emissions are linked with decreases in stomatal conductance.

Thus, declines in methanol emissions in the afternoon could be attributed to both reductions in growth rates as well as reduced stomatal conductance. Taken together, the results are therefore consistent with the idea that growth is much more sensitive to mild tissue water stress than photosynthesis[12] with growth being one of the first major physiological processes to be downregulated, potentially mediated by upregulation of pectin methyl esterase inhibitor (PMEI) enzyme activity[29,30]. These results suggest a model of hydraulically-driven methanol emissions and growth rates at night; and temperature stimulated (morning), followed by potentially inhibited (afternoon) methanol emission and growth processes during the day (supplementary **Figure S17**). Thus, these findings support the emerging view of methanol emissions as a chemical biomarker of primary cell wall growth, often difficult to detect by physical means on short time scales (i.e. < 24 hours) due to large diurnal changes in tissue water status[12]. These results are consistent with the view of pectin methyl ester hydrolysis and methanol emissions tightly linked with changes in primary cell wall elasticity and growth (see supplementary information content, 'Pectin demethylation, methanol emissions, and growth') and highlights the potential for methanol emissions as a non-invasive chemical tracer of plant water status and growth processes across temporal and spatial scales.

Supplementary Figures

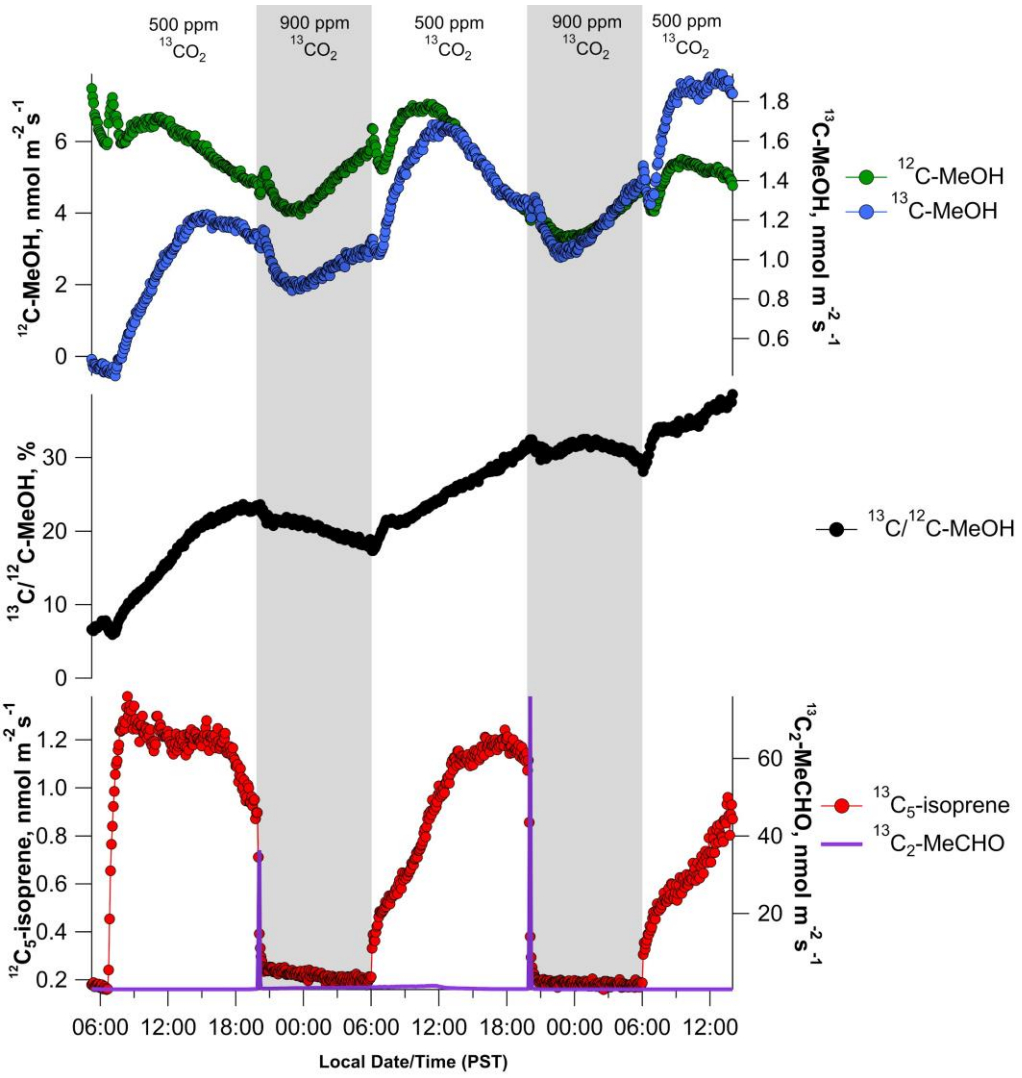

Figure S1: Biological replicates #1 of 2-day time series in a 21% O_2 atmosphere showing dynamic branch labeling of methanol emissions via the photosynthetic-C_1 pathway under elevated $^{13}CO_2$. Night periods are shaded in gray.

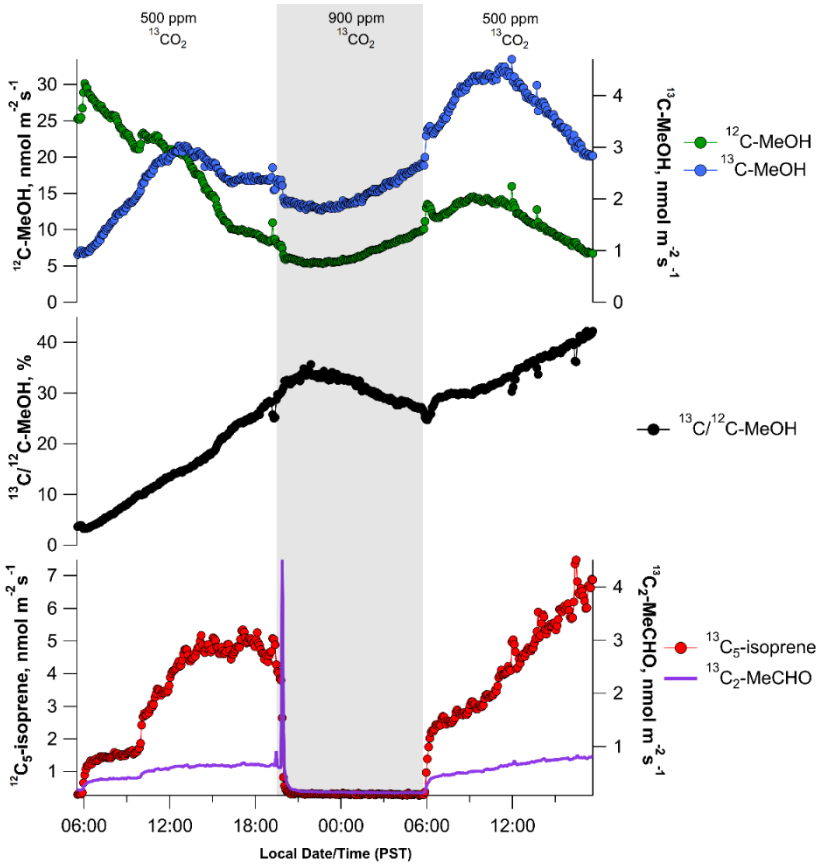

Figure S2: Biological replicates #2 of 2-day time series in a 21% O_2 atmosphere showing dynamic branch labeling of methanol emissions via the photosynthetic-C_1 pathway under elevated $^{13}CO_2$. Night periods are shaded in gray.

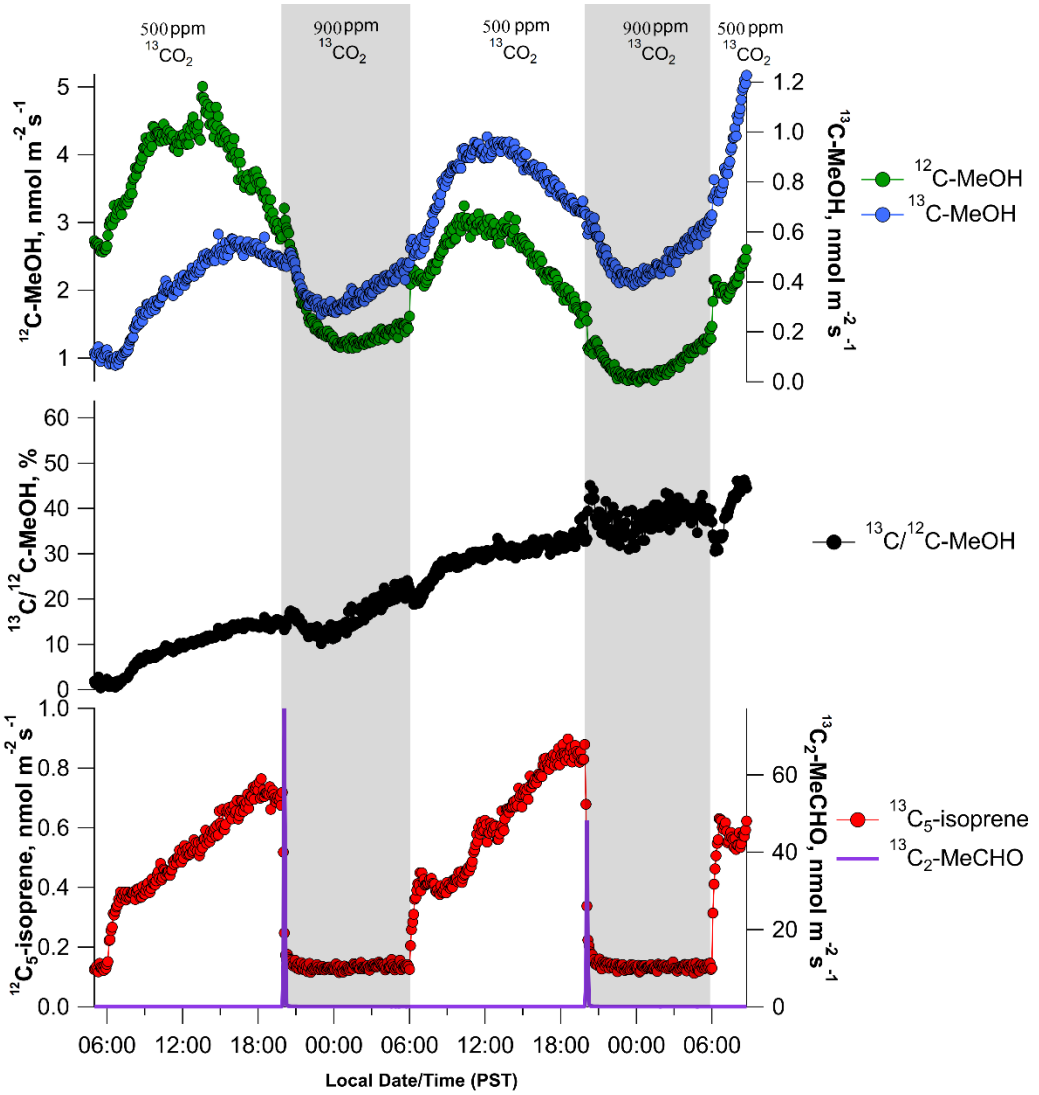

Figure S3: Biological replicates #3 of 2-day time series in a 21% O_2 atmosphere showing dynamic branch labeling of methanol emissions via the photosynthetic-C_1 pathway under elevated $^{13}CO_2$. Night periods are shaded in gray.

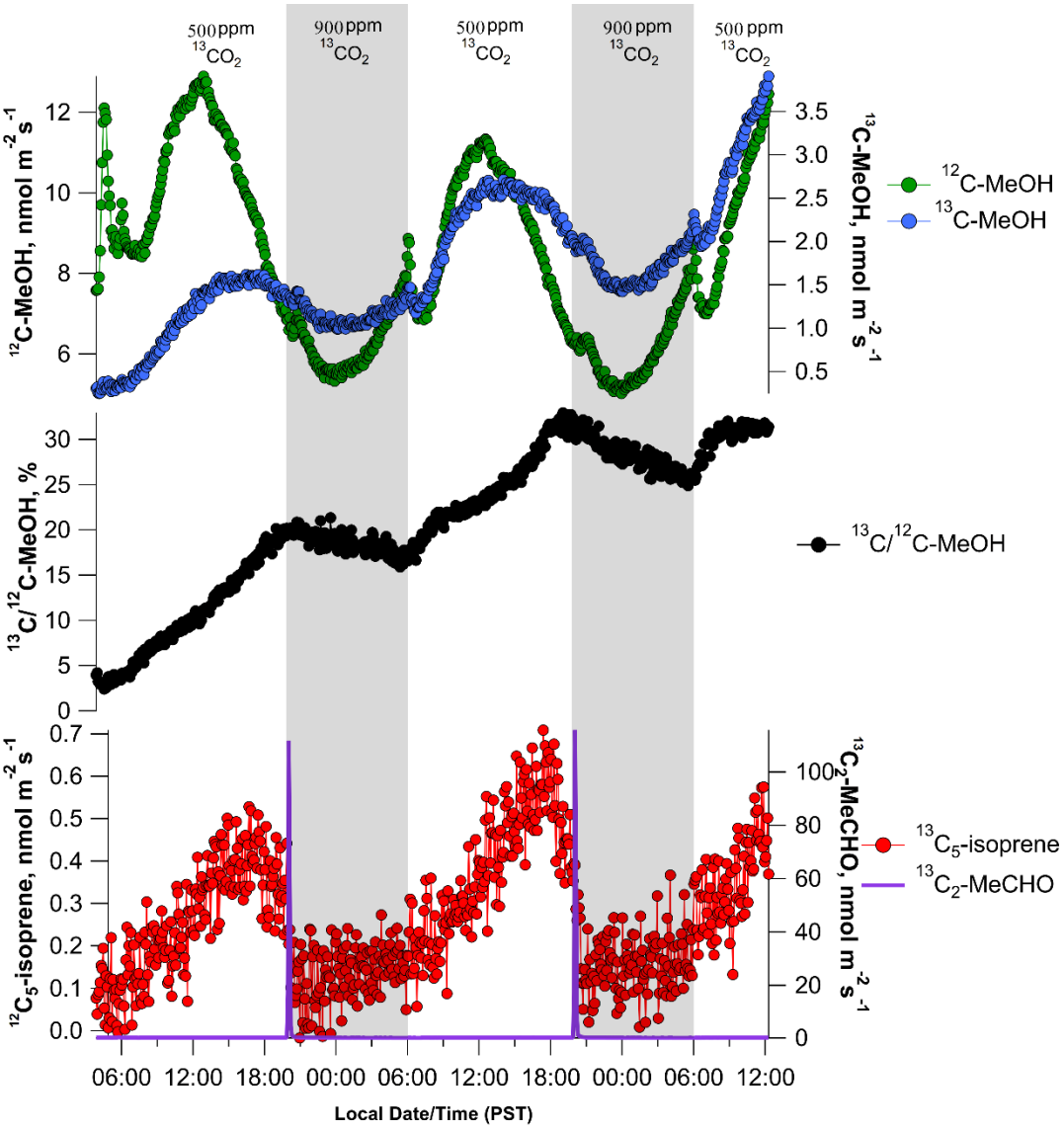

Figure S4: Biological replicates #4 of 2-day time series in a 21% O_2 atmosphere showing dynamic branch labeling of methanol emissions via the photosynthetic-C_1 pathway under elevated $^{13}CO_2$. Night periods are shaded in gray.

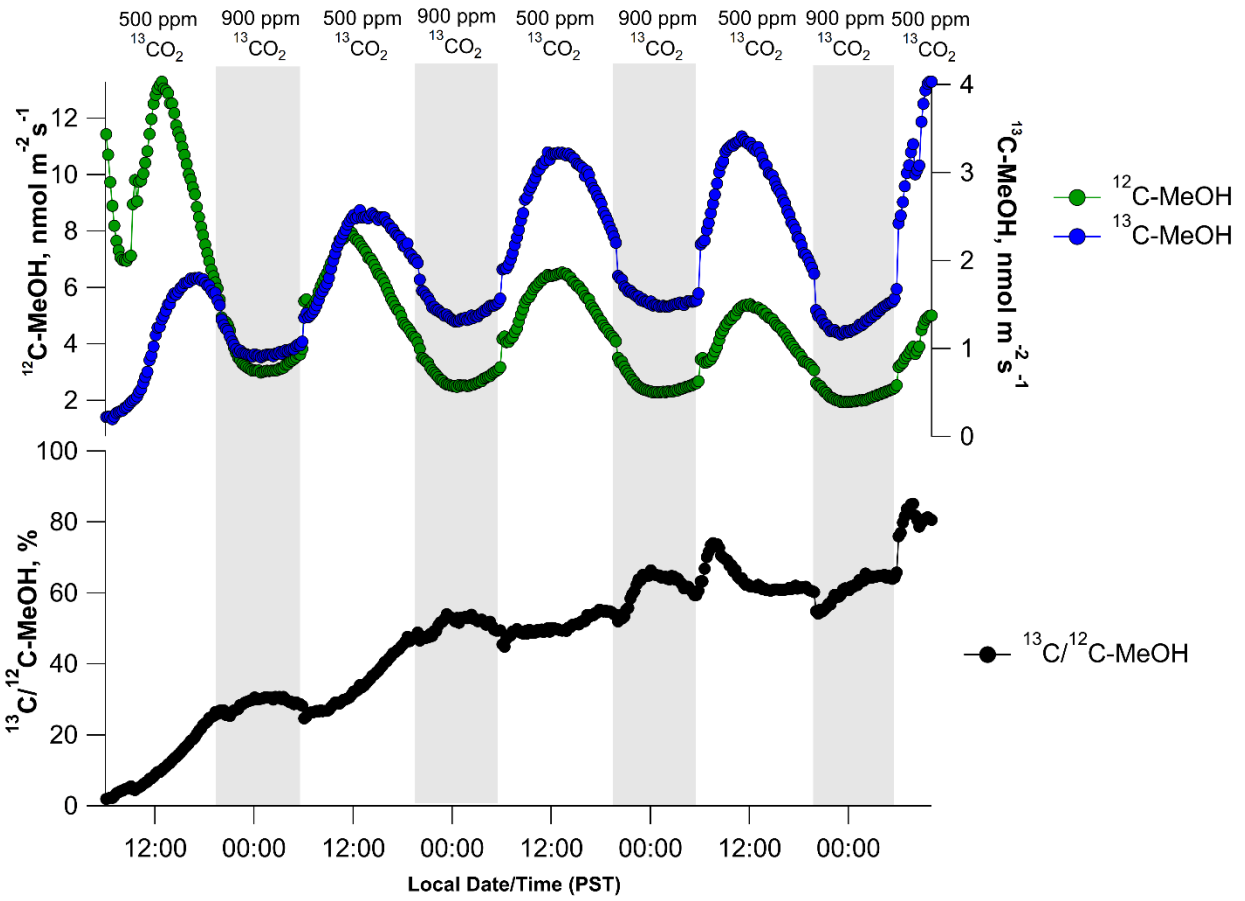

Figure S5: 5-day time series in a 21% O_2 atmosphere showing dynamic branch labeling of methanol emissions via the photosynthetic-C_1 pathway under elevated $^{13}CO_2$. Night periods are shaded in gray.

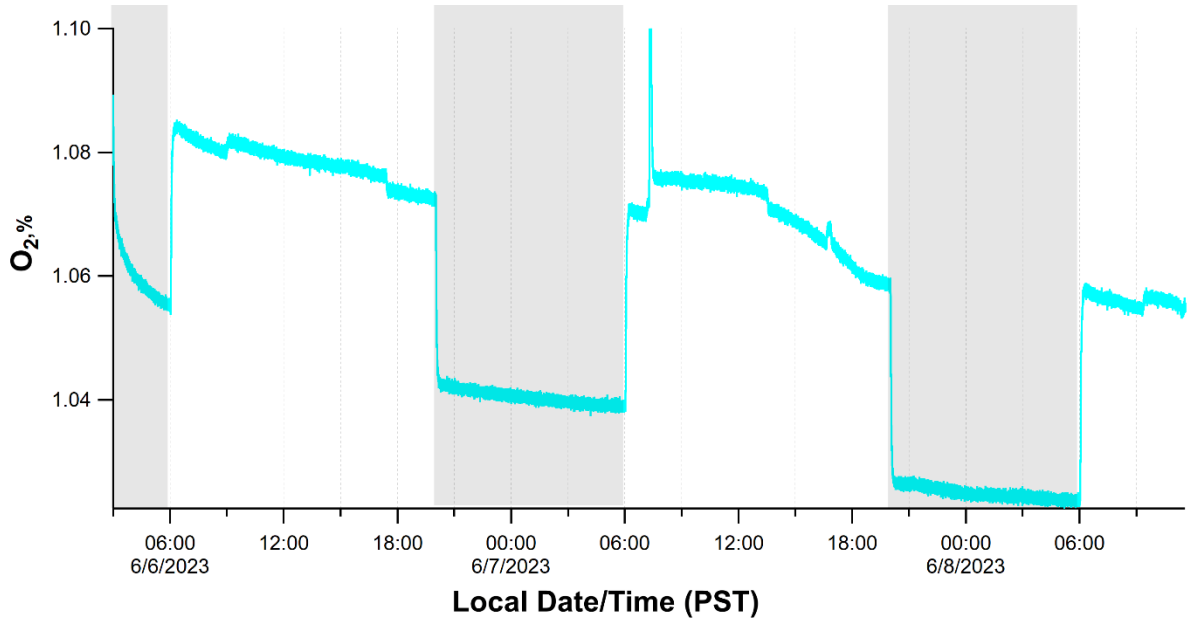

Figure S6: 2-day CRDS O_2 concentration time series data during branch $^{13}CO_2$ labeling under a 1% O_2 atmosphere. The light regions represent the day (>600 ppm $^{13}CO_2$) and the shaded regions represent the night (~1000 ppm $^{13}CO_2$). The observations verify that despite the branch being exposed to a 1% O_2 atmosphere, net photosynthetic O_2 production is detected in the light.

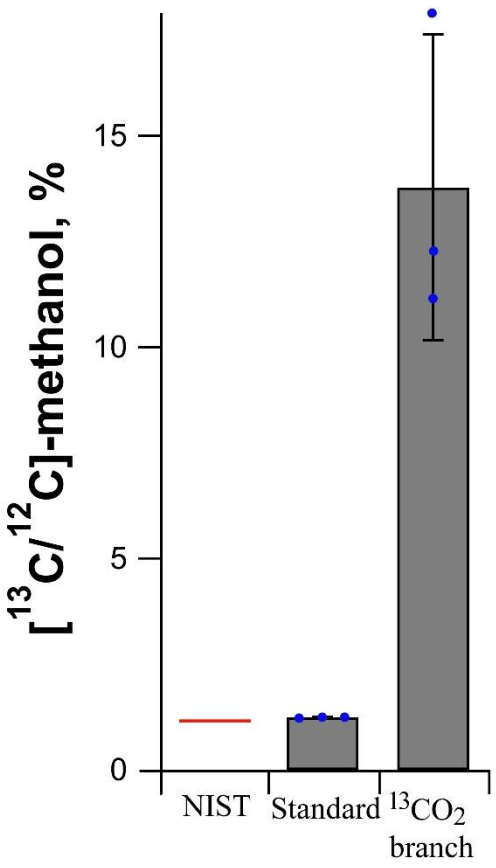

Figure S7: TD-GC-MS analysis of the methanol peak at retention time 7.7-7.8 min following branch photosynthesis under a $^{13}CO_2$ atmosphere. [$^{13}C/^{12}C$]-methanol ratio (%) was calculated from Japan AIST/NIMC Database (Spectrum MS-NW-72), accessed via the NIST mass spectral database (NIST MS number 229809, Collection (C) 2014) plotted as a red line, from a methanol gas phase standard (n = 3), and from branch headspace air samples (n = 3) collected following 3 hr of photosynthesis under $^{13}CO_2$ labelling in the light.

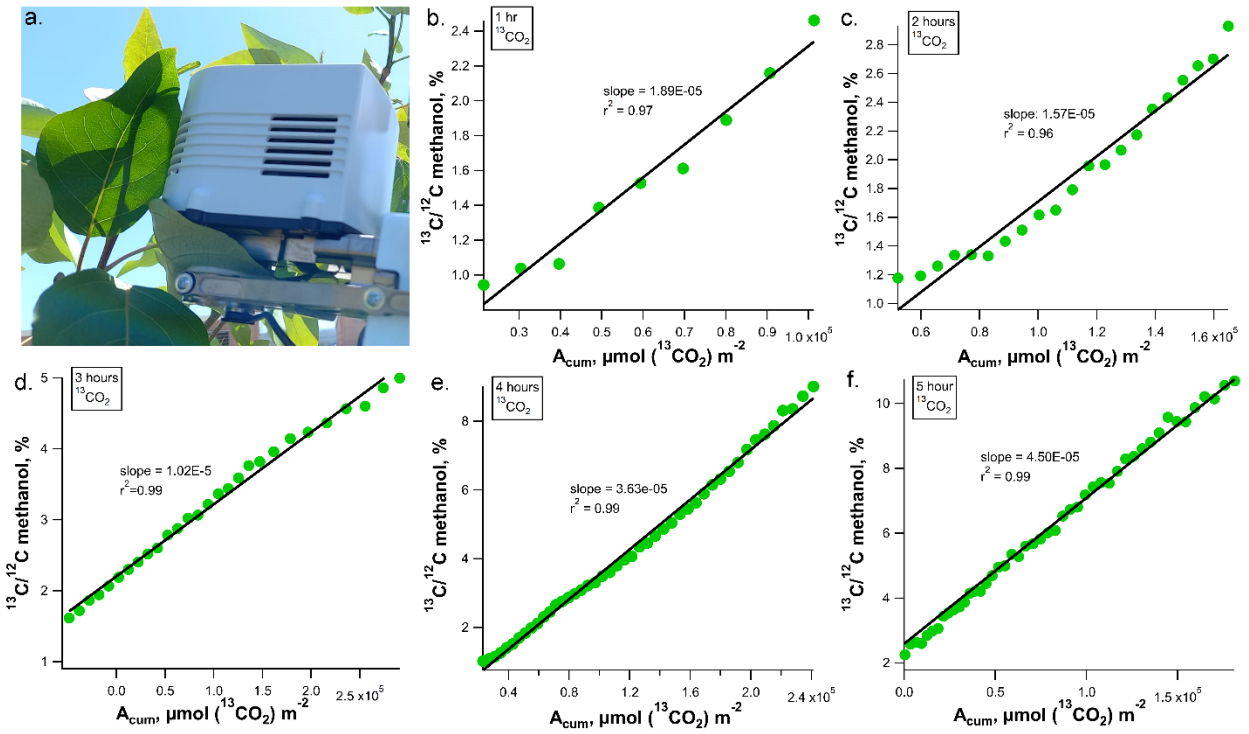

Figure S8: Example tight linear correlations between instantaneous $^{13}C/^{12}C$-methanol emission ratio and cumulative photosynthesis of $^{13}CO_2$ for *P. trichocharpa* leaves under constant environmental conditions in the light using (**a.**) a leaf chamber for (**b.**)1 hr, (**c.**) 2 hr, (**d.**) 3 hr, (**e.**) 4 hr, and (**f.**) 5 hr.

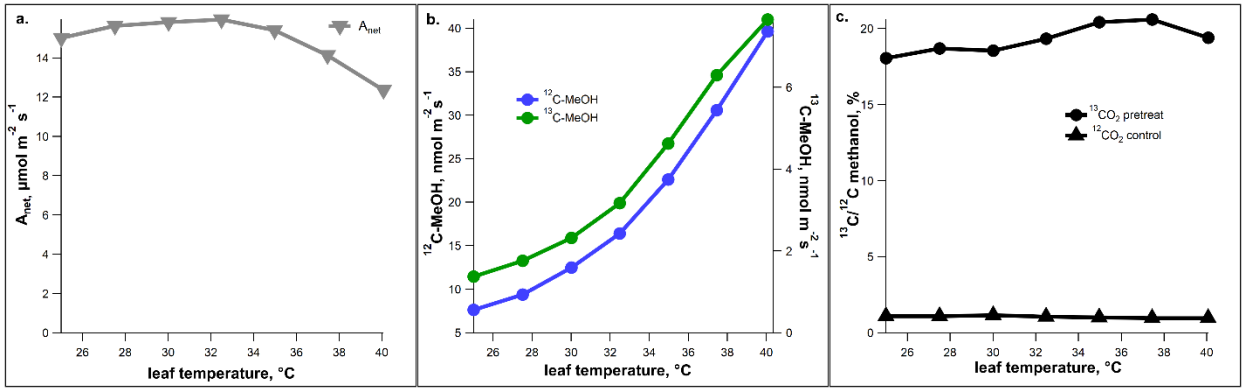

Figure S9: Example leaf gas exchange responses to temperature under a constant leaf chamber headspace concentration of $^{12}CO_2$ (400 ppm), following two day/night light cycles under a $^{13}CO_2$ atmosphere. Note the strong temperature stimulated emission of ^{12}C- and ^{13}C- methanol, but with a relatively constant $^{13}C/^{12}C$-methanol ratio highly enriched in ^{13}C relative to the $^{12}CO_2$ control.

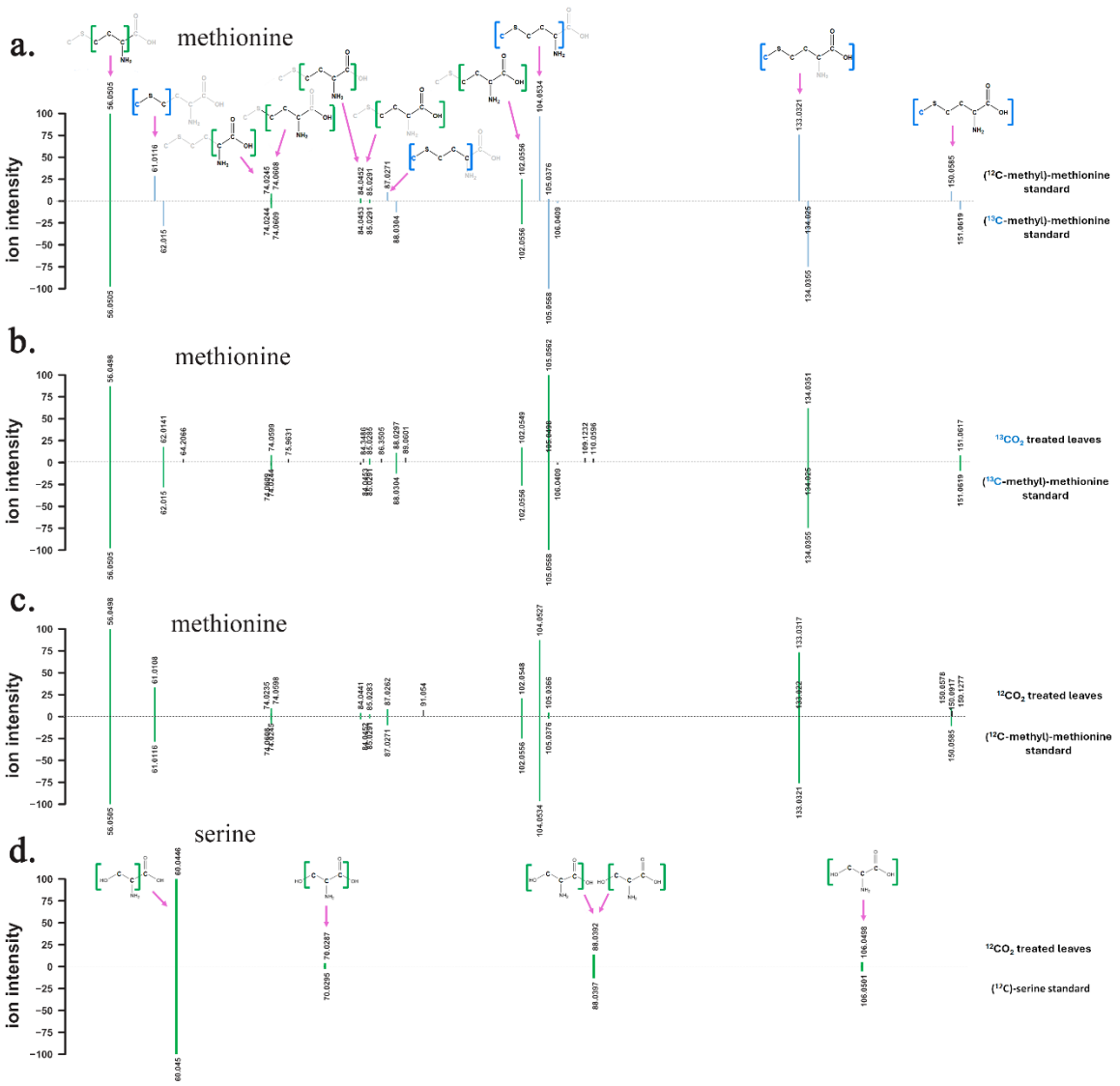

Figure S10: LC-MS/MS ^{13}C-labelling analysis of methionine and serine extracted from *P. trichocarpa* leaves following 2-day gas exchange studies under a $^{12}CO_2$ or $^{13}CO_2$ atmosphere with 21% O_2. (**a.**) Methionine mirror plots comparing fragmentation patterns from a (^{12}C-methyl)-methionine reference standard and a (^{13}C-methyl)-methionine reference standard, and (**b.**) Methionine mirror plots comparing fragmentation patterns of a $^{13}CO_2$-treated poplar leaf and a (^{13}C-methyl)-methionine reference standard, (**c.**) Methionine mirror plots comparing fragmentation patterns of a $^{12}CO_2$-treated poplar leaf and a (^{12}C-methyl)-methionine reference standard. (**d.**) Methionine mirror plots comparing fragmentation patterns of a $^{12}CO_2$-treated poplar leaf and a (^{12}C-methyl)-methionine reference standard. The carbon atoms of the methionine and serine molecules within each fragment are shown as previously determined[31]. Green fragments indicate matching ions within 15 ppm and blue fragments indicate that the lower ion is within 15ppm of the expected ^{13}C-labeled fragment isotopologue.

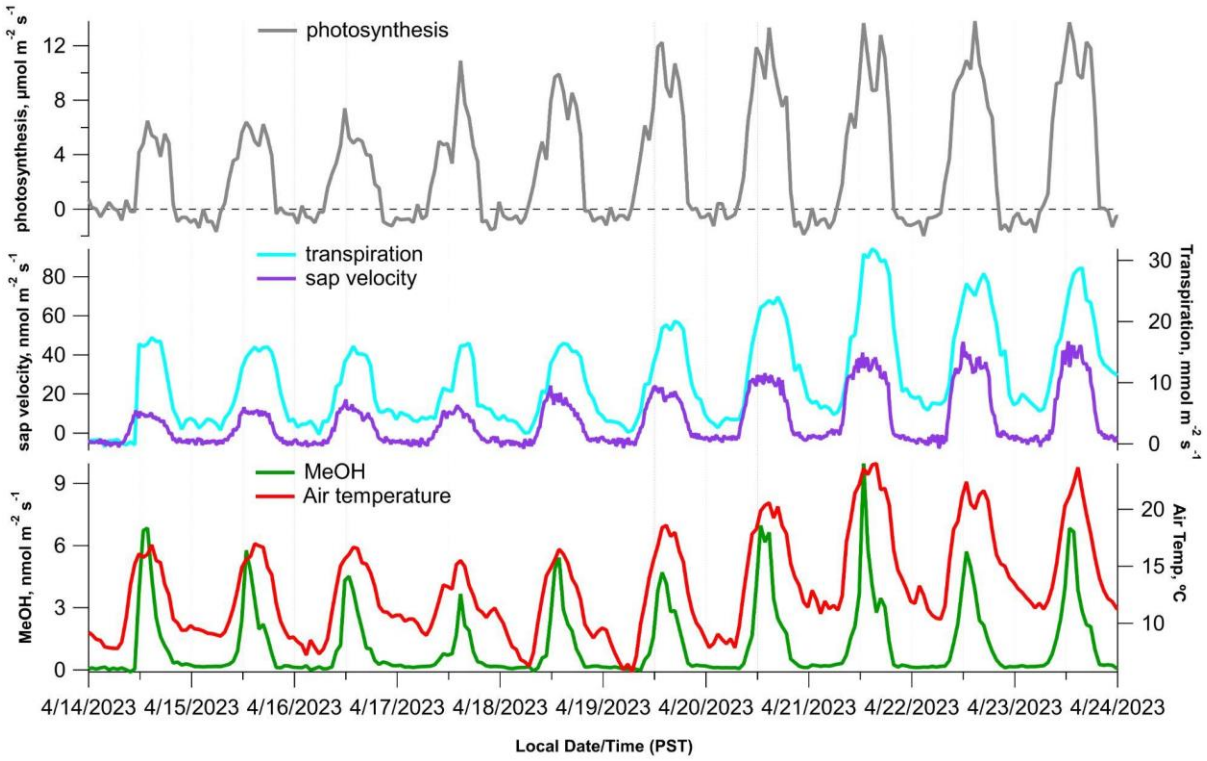

Figure S11: Time series plot in April 2023 showing the diurnal variations of branch photosynthesis, transpiration, and methanol (CH_3OH) emissions of a *P. trichocarpa* individual. Also shown are time series data of sap velocity from a different *P. trichocarpa* individual as well as air temperature.

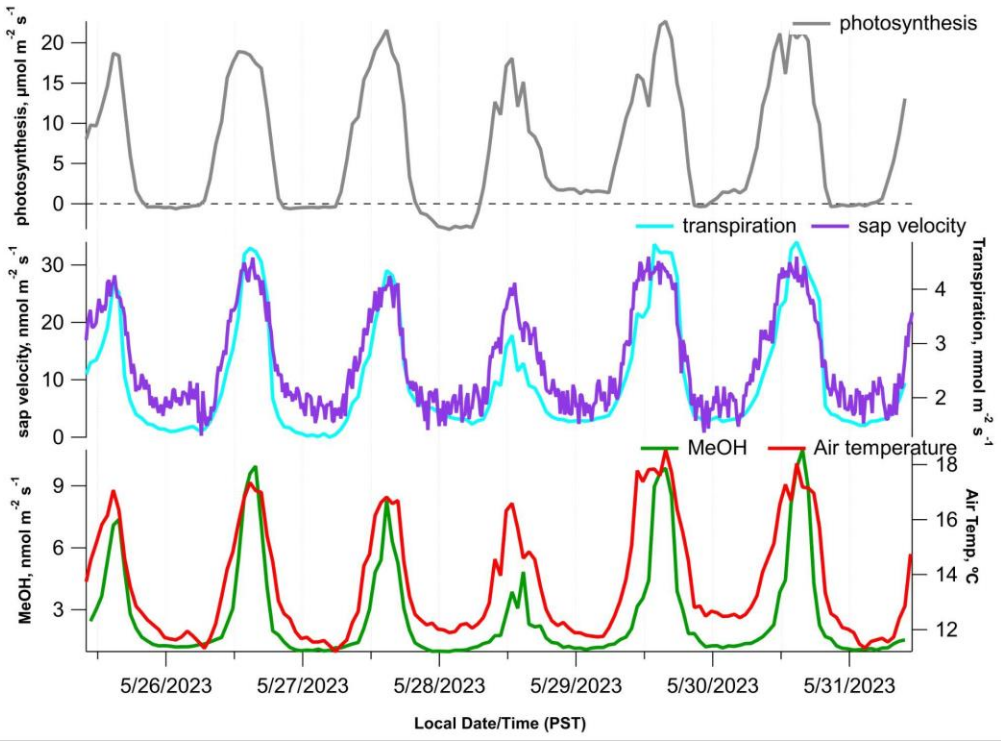

Figure S12: Time series plot in May 2023 showing the diurnal variations of branch photosynthesis, transpiration, and methanol (CH_3OH) emissions of a *P. trichocarpa* individual. Also shown are time series data of sap velocity from a different *P. trichocarpa* individual as well as air temperature.

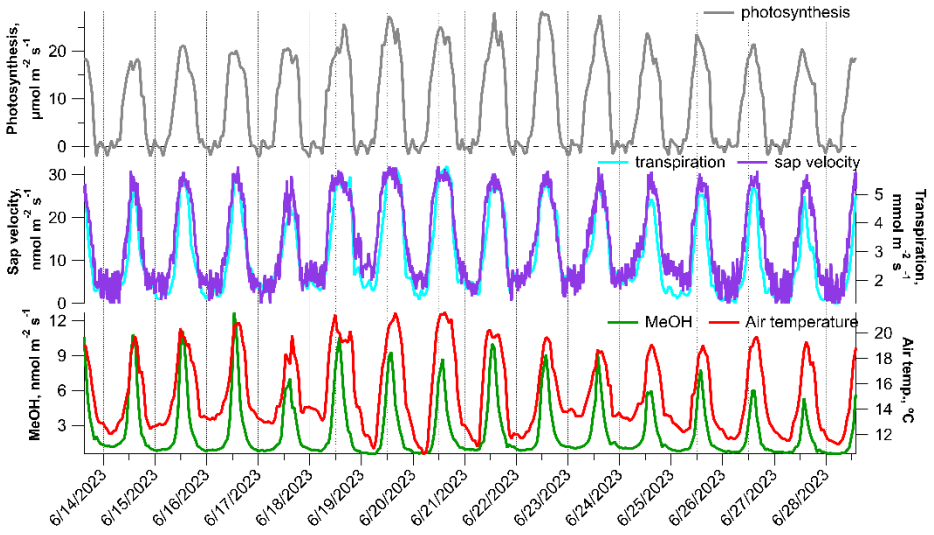

Figure S13: Time series plot in June 2023 showing the diurnal variations of branch photosynthesis, transpiration, and methanol (CH_3OH) emissions of a *P. trichocarpa* individual. Also shown are time series data of sap velocity from a different *P. trichocarpa* individual as well as air temperature.

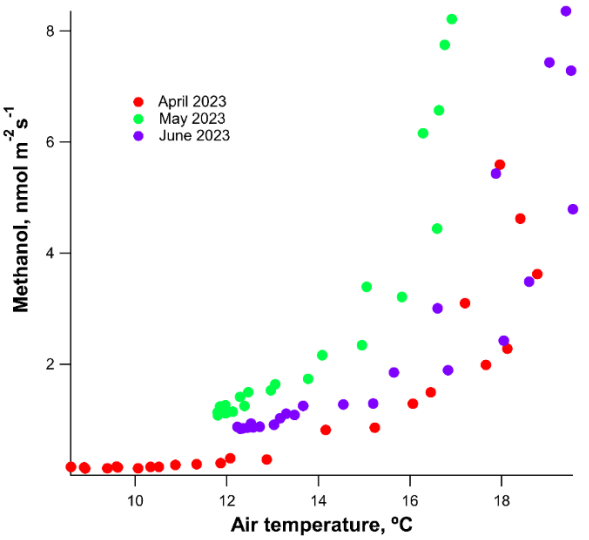

Figure S14: Scatter plot of methanol (CH_3OH) branch emissions from a *P. trichocarpa* individual in the Berkeley, CA, USA field site versus air temperature during April, May, and June 2023.

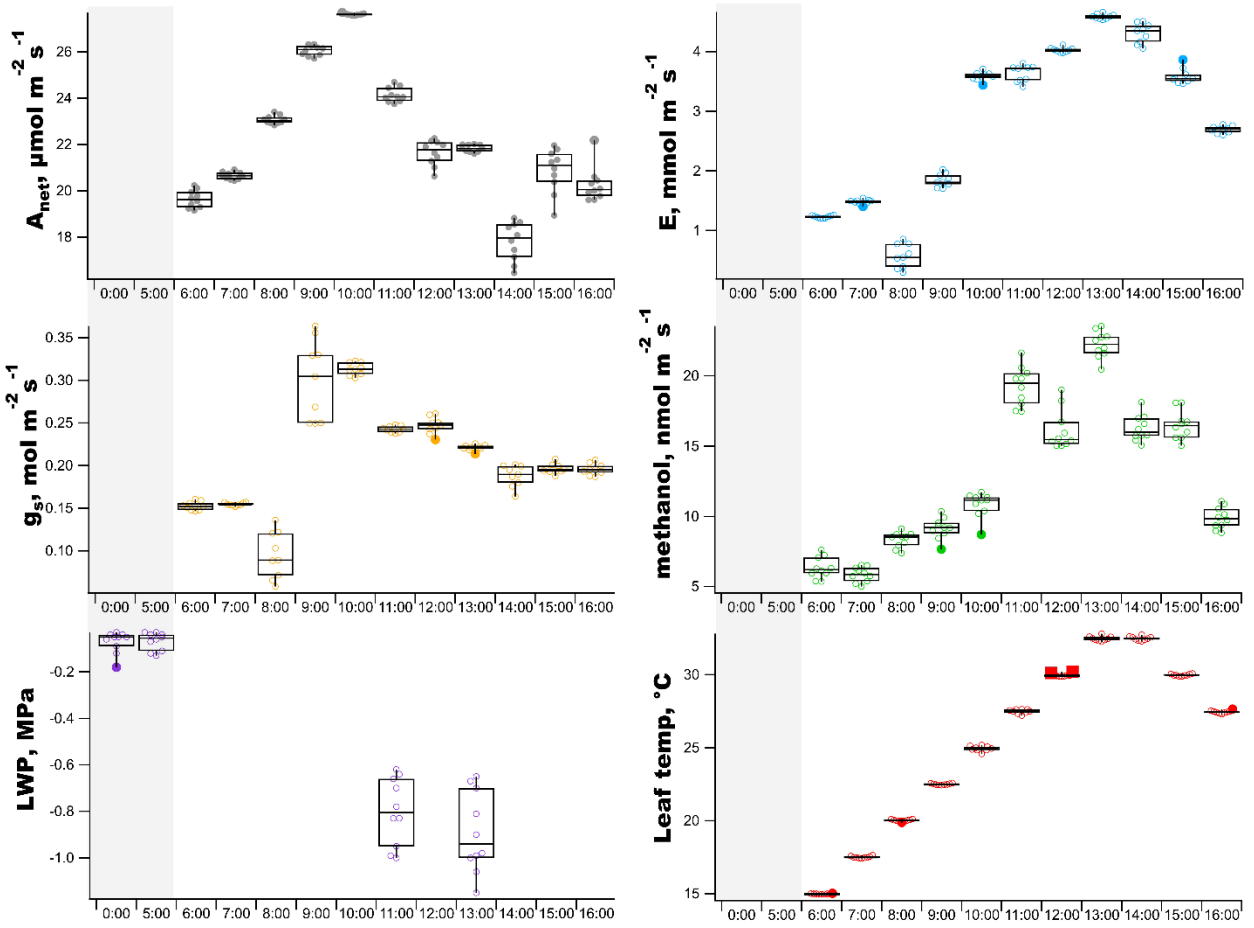

Figure S15: Time series plot showing the diurnal variation of leaf photosynthesis (A_{net}), stomatal conductance (gs), and water potential (LWP), together with leaf transpiration (E), methanol emissions (CH_3OH), and leaf temperature versus hour of the day from the canopy of a *Populus trichocarpa* individual at the Berkeley, CA field site during the early growing season (April 2023). Leaf gas exchange measurements were collected under constant light, CO_2 concentration, and reference humidity, but with varying leaf temperature. The shaded region indicates the night period. Individual data points (colored dots) represent raw measurements (10 measurements per leaf). The boxes show the interquartile range (IQR), with the line inside the box indicating the median. The whiskers represent the variability of the data, and the error bars denote the standard deviation (SD) for each time period. LWP was collected only at 00:00 (midnight), 5:00 (predawn), 12:00 (noon), and 14:00 (early afternoon), whereas leaf gas exchange measurements were collected throughout the light period (6:00–16:00).

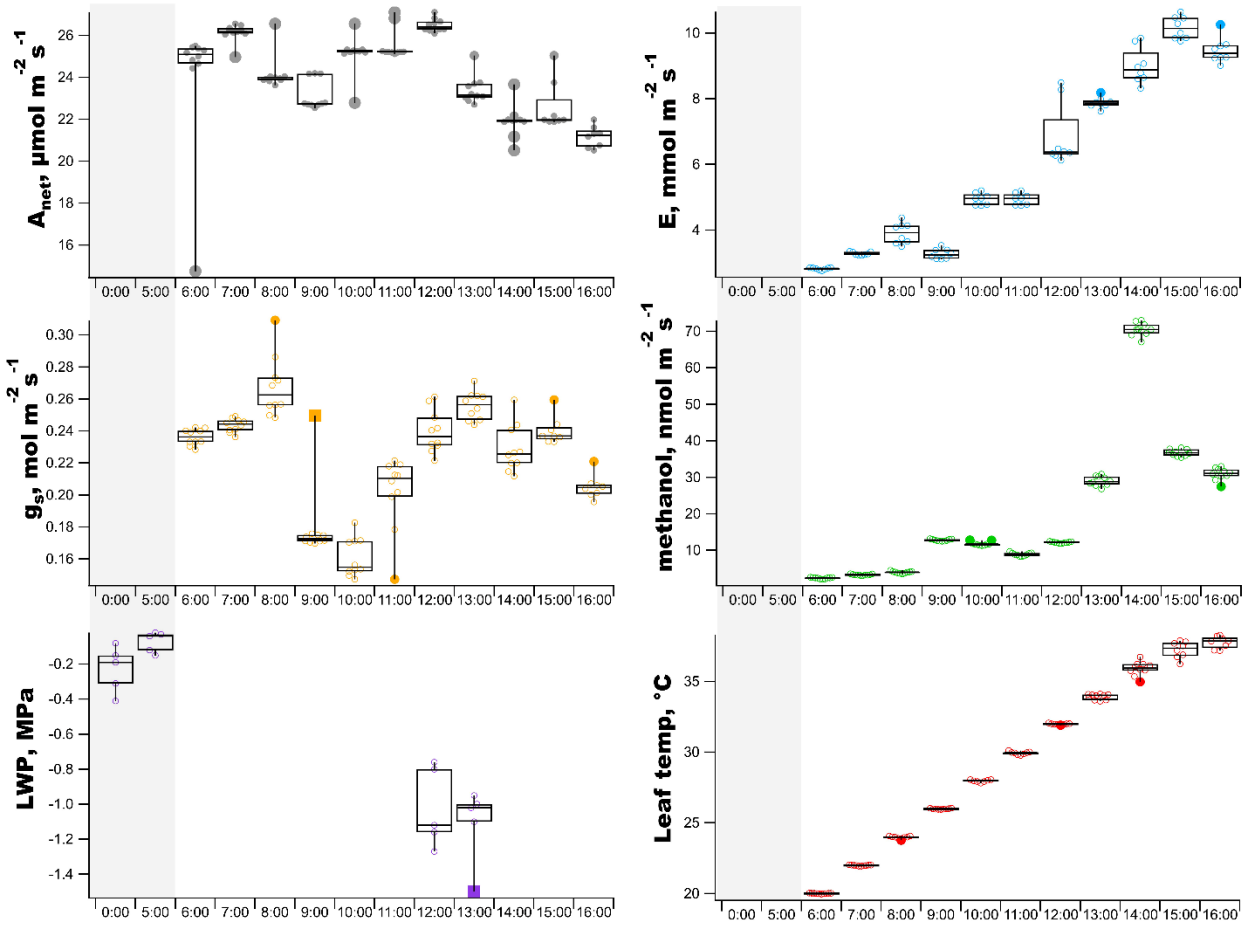

Figure S16: Time series plot showing the diurnal variation of leaf photosynthesis (A_{net}), stomatal conductance (gs), and water potential (LWP), together with leaf transpiration (E), methanol emissions (CH_3OH), and leaf temperature versus hour of the day from the canopy of a *Populus trichocarpa* individual at the Berkeley, CA field site during the mid growing season (June 2023). Leaf gas exchange measurements were collected under constant light, CO_2 concentration, and reference humidity, but with varying leaf temperature. The shaded region indicates the night period. Individual data points (colored dots) represent raw measurements (10 measurements per leaf). The boxes show the interquartile range (IQR), with the line inside the box indicating the median. The whiskers represent the variability of the data, and the error bars denote the standard deviation (SD) for each time period. LWP was collected only at 00:00 (midnight), 5:00 (predawn), 12:00 (noon), and 14:00 (early afternoon), whereas leaf gas exchange measurements were collected throughout the light period (6:00–16:00).

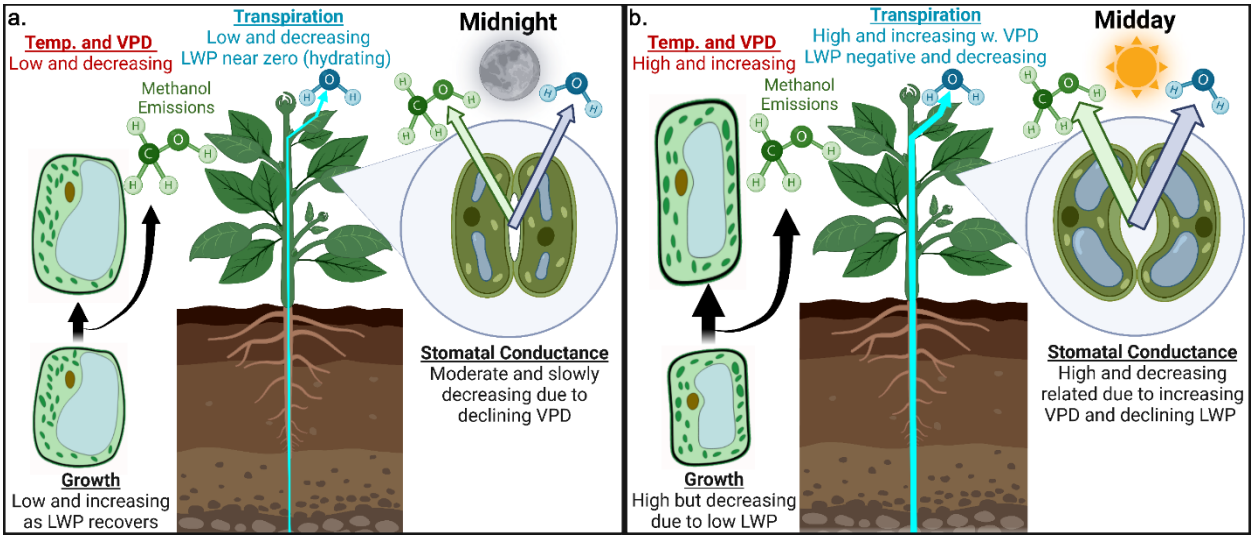

Figure S17: Graphical representation of diurnal growth and methanol emission processes in plants. **a**. Midnight starts the accelerating growth phase through recovery of tissue water potential (i.e. leaf water potential, LWP) resulting in a hydraulically-driven increase of nocturnal growth rates and methanol emissions. **b**. Midday starts the deaccelerating growth phase characterized by increasing leaf tissue water stress, and decreasing growth and methanol emission rates. Temperature (Temp.) drives plant transpiration through a strong impact on the leaf-to-atmosphere vapor pressure deficit (VPD).
Created in BioRender. Jardine, K. (2024) *BioRender.com/r65a877*

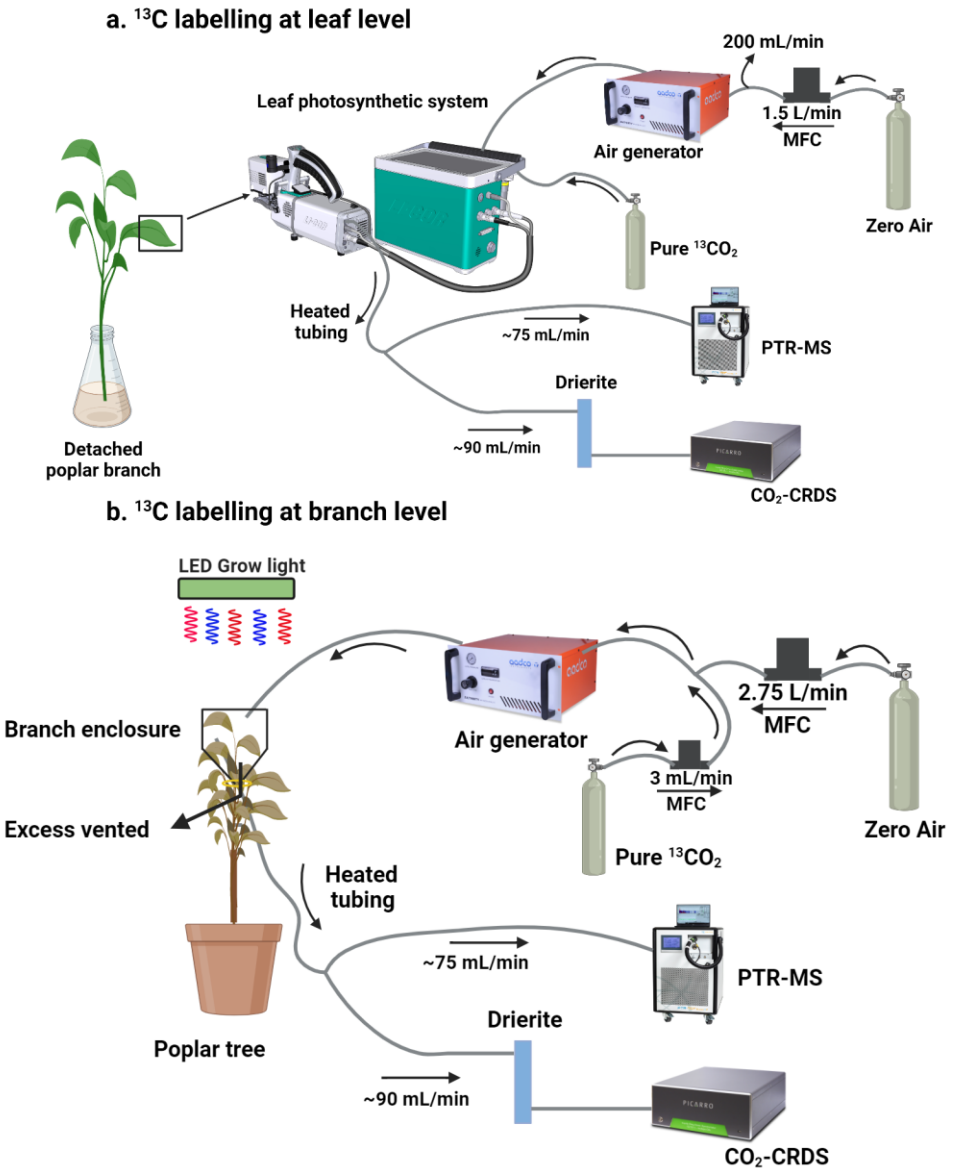

Figure S18: Graphical summary of gas exchange methods used during $^{13}CO_2$ labelling of the photosynthetic C_1 pathway in *P. trichocharpa* leaves at the (**a.**) leaf level on detached and hydrated branches lasting 1-5 hr and (**b.**) branch level using potted plants lasting 2-5 days. *Created in BioRender. K. Jardine (2024)* BioRender.com/d79c177

Supplementary References

1 Peaucelle, A. *et al.* Pectin-induced changes in cell wall mechanics underlie organ initiation in Arabidopsis. *Current biology* **21**, 1720-1726 (2011).

2 Peaucelle, A. *et al.* Arabidopsis phyllotaxis is controlled by the methyl-esterification status of cell-wall pectins. *Current Biology* **18**, 1943-1948 (2008).

3 Peaucelle, A., Braybrook, S. & Höfte, H. Cell wall mechanics and growth control in plants: the role of pectins revisited. *Frontiers in plant science* **3**, 121 (2012).

4 Haas, K. T., Wightman, R., Meyerowitz, E. M. & Peaucelle, A. Pectin homogalacturonan nanofilament expansion drives morphogenesis in plant epidermal cells. *Science* **367**, 1003-1007 (2020).

5 O'NEILL, M., Albersheim, P. & Darvill, A. in *Methods in plant biochemistry* Vol. 2 415-441 (Elsevier, 1990).

6 Hüve, K. *et al.* Simultaneous growth and emission measurements demonstrate an interactive control of methanol release by leaf expansion and stomata. *Journal of experimental botany* **58**, 1783-1793 (2007).

7 Nemecek-Marshall, M., MacDonald, R. C., Franzen, J. J., Wojciechowski, C. L. & Fall, R. Methanol emission from leaves (enzymatic detection of gas-phase methanol and relation of methanol fluxes to stomatal conductance and leaf development). *Plant Physiology* **108**, 1359-1368 (1995).

8 Jardine, K. J. *et al.* Methanol and isoprene emissions from the fast growing tropical pioneer species Vismia guianensis (Aubl.) Pers.(Hypericaceae) in the central Amazon forest. *Atmospheric Chemistry and Physics* **16**, 6441-6452 (2016).

9 Jacob, D. J. *et al.* Global budget of methanol: Constraints from atmospheric observations. *Journal of Geophysical Research: Atmospheres* **110** (2005).

10 Jardine, K. *et al.* Cell wall ester modifications and volatile emission signatures of plant response to abiotic stress. *Plant, Cell & Environment* **45**, 3429-3444 (2022).

11 Jardine, K. *et al.* Dynamic balancing of isoprene carbon sources reflects photosynthetic and photorespiratory responses to temperature stress. *Plant physiology* **166**, 2051-2064 (2014).

12 Zweifel, R. *et al.* Why trees grow at night. *New Phytologist* **231**, 2174-2185 (2021).

13 Jardine, K., Wegener, F., Abrell, L., Van Haren, J. & Werner, C. Phytogenic biosynthesis and emission of methyl acetate. *Plant, cell & environment* **37**, 414-424 (2014).

14 Harley, P., Greenberg, J., Niinemets, Ü. & Guenther, A. Environmental controls over methanol emission from leaves. *Biogeosciences* **4**, 1083-1099 (2007).

15 Roje, S. *et al.* Isolation, characterization, and functional expression of cDNAs encoding NADH-dependent methylenetetrahydrofolate reductase from higher plants. *Journal of Biological Chemistry* **274**, 36089-36096 (1999).

16 Gorelova, V. *et al.* Evolution of folate biosynthesis and metabolism across algae and land plant lineages. *Scientific Reports* **9**, 5731 (2019).

17 Bedhomme, M. *et al.* Folate metabolism in plants: an Arabidopsis homolog of the mammalian mitochondrial folate transporter mediates folate import into chloroplasts. *Journal of Biological Chemistry* **280**, 34823-34831 (2005).

18 Ravanel, S. *et al.* Methionine metabolism in plants: chloroplasts are autonomous for de novo methionine synthesis and can import S-adenosylmethionine from the cytosol. *Journal of Biological Chemistry* **279**, 22548-22557 (2004).

19 Moffatt, B. A. & Weretilnyk, E. A. Sustaining S-adenosyl-l-methionine-dependent methyltransferase activity in plant cells. *Physiologia Plantarum* **113**, 435-442 (2001).

20 Klimašauskas, S. & Weinhold, E. A new tool for biotechnology: AdoMet-dependent methyltransferases. *Trends in biotechnology* **25**, 99-104 (2007).

21 Keppler, F., Kalin, R., Harper, D., McRoberts, W. & Hamilton, J. T. Carbon isotope anomaly in the major plant C 1 pool and its global biogeochemical implications. *Biogeosciences* **1**, 123-131 (2004).
22 Brugnoli, E. & Farquhar, G. D. in *Photosynthesis: physiology and metabolism* 399-434 (Springer, 2000).
23 Jiang, T. *et al.* Theoretical analysis of the kinetic isotope effect on carboxylation in RubisCO. *Journal of Computational Chemistry* **41**, 1116-1123 (2020).
24 Romek, K. M. *et al.* Insights into the role of methionine synthase in the universal 13C depletion in O-and N-methyl groups of natural products. *Archives of biochemistry and biophysics* **635**, 60-65 (2017).
25 Zierer, W. *et al.* Phloem-specific methionine recycling fuels polyamine biosynthesis in a sulfur-dependent manner and promotes flower and seed development. *Plant physiology* **170**, 790-806 (2016).
26 Bourgis, F. *et al.* S-methylmethionine plays a major role in phloem sulfur transport and is synthesized by a novel type of methyltransferase. *The Plant Cell* **11**, 1485-1497 (1999).
27 Garneau, M. G., Lu, M.-Z., Grant, J. & Tegeder, M. Role of source-to-sink transport of methionine in establishing seed protein quantity and quality in legumes. *Plant Physiology* **187**, 2134-2155 (2021).
28 Jardine, K. J. *et al.* Cell wall ester modifications and volatile emission signatures of plant response to abiotic stress. *Plant, Cell & Environment* **45**, 3429-3444 (2022).
29 Wang, J., Ling, L., Cai, H. & Guo, C. Gene-wide identification and expression analysis of the PMEI family genes in soybean (Glycine max). *3 Biotech* **10**, 1-19 (2020).
30 Wormit, A. & Usadel, B. The multifaceted role of pectin methylesterase inhibitors (PMEIs). *International journal of molecular sciences* **19**, 2878 (2018).
31 Zhang, P. *et al.* Revisiting fragmentation reactions of protonated α-amino acids by high-resolution electrospray ionization tandem mass spectrometry with collision-induced dissociation. *Scientific reports* **9**, 6453 (2019).